

provides a scattering power of 0.28 electron per cubic angstrom. Given a numerical aperture of 1/25 and $\lambda = 24.7 \text{ \AA}$, we can calculate that the resolution cell, which is an ellipsoid of revolution with semiaxes 377, 377, and 9417 \AA , contains a scattering power of $n_e = 7.1 \times 10^8$ electrons that will scatter coherently. By use of the Thomson cross section at small angles and defining the contrast as $(I_{\max} - I_{\min}) / (I_{\max} + I_{\min})$, where I_{\max} and I_{\min} are the maximum and minimum intensity, respectively, of the fringe pattern, we find that for the case of a strong reference beam the contrast is given by $2r_0 n_e / f$, where f is the sample-to-hologram distance and r_0 is the classical electron radius. Setting $f = 400 \text{ \mu m}$ and $r_0 = 2.818 \times 10^{-5} \text{ \AA}$, we obtain the value 0.01 for the contrast. Bearing in mind that the process of glancing incidence shadowing amplifies the contrast considerably, this is consistent with our observations.

23. These visual observations have been confirmed by computer analysis of a digitized form of the hologram in Fig. 2B. The power spectral density of linear scans across the electron micrograph is observed to fall off approximately as the inverse of the spatial

frequency, until it flattens out to white noise. Although we have yet to determine the acceptable signal-to-noise ratio for hologram reconstruction, the transition from usable signal into noise appears to occur at a spatial frequency between 25 and 50 μm^{-1} . We therefore consider that our visual estimate of 16 μm^{-1} is a safe choice for a working value of the maximum useful frequency of the hologram.

24. G. Liu and P. D. Scott, *J. Opt. Soc. Am. A* **4**, 159 (1987).
 25. We acknowledge valuable help and advice from J. Boland, M. Caldarolo, K. Conkling, C. Dittmore, T. Ermak, J. Grendell, D. Joel, H. Rarback, and D. Sayre, as well as the generous assistance of the staff at the NSLS. We also acknowledge the support of the National Science Foundation under grant BBS-8618066 (C.J. and J.K.) and the Department of Energy under contract DE-AC03-76SF00098 (M.H.). This work was carried out in part at the NSLS, which is supported by the Department of Energy under contract DE-AC02-76CH00016.

7 May 1987; accepted 1 September 1987

Demonstration of X-ray Holography with an X-ray Laser

JAMES E. TREBES, STEVEN B. BROWN, E. MICHAEL CAMPBELL, DENNIS L. MATTHEWS, DAVID G. NILSON, GARY F. STONE, DAVID A. WHELAN

An x-ray hologram was made by means of an x-ray laser and a laser-quality near normal incidence x-ray mirror. The high brightness and large coherence lengths of x-ray lasers now offer the potential for in vitro three-dimensional high-resolution holographic images of dynamically varying biological microstructures.

X-RAY HOLOGRAPHY OFFERS THE POTENTIAL for obtaining high-resolution three-dimensional images of in vitro biological microstructures. Significant progress toward this goal has been achieved with holography systems using synchrotron x-ray sources (1) and recently spatial resolutions as small as 40 nm have been demonstrated (2). These experiments required x-ray exposures of an hour or longer, which makes high spatial resolution difficult to achieve in live biological specimens because of blurring of the image. This blurring is caused by specimen motion and will prohibit the imaging of dynamical processes within the specimen. A possible solution to this problem is to exploit the high brightness and long coherence lengths produced by x-ray lasers; the hologram could then be made with exposure times of less than 1 nsec. This report presents the results from an experiment in which an x-ray laser was used to produce x-ray holograms. The holography geometry used was a Gabor (3) in-line type modified by the inclusion of a high reflectivity multilayer x-ray mirror (4) used as a narrow bandpass filter. The x-ray mirror had a flatness and roughness of less than $\lambda/100$

(where λ is the wavelength) at the x-ray laser wavelengths.

The soft x-ray laser used in these experiments was the neon-like selenium (ionized 24 times) laser produced at the Lawrence Livermore National Laboratory (LLNL) Nova Laser Two-Beam Facility (5). The x-ray laser emission occurs when two of the Nova laser's ten beams are focused onto a thin selenium and plastic foil in a line focus. These beams produce an intensity on the foil of $6 \times 10^{13} \text{ W/cm}^2$, creating the electron temperature ($\sim 1000 \text{ eV}$) and density ($> 10^{20}$ electrons per cubic centimeter) necessary for lasing. The dominant laser emission is at 20.6 and 20.9 nm with a maximum total output power of approximately 5 MW in a 200-psec pulse. The x-ray lasers used in these experiments were operated at about 500 kW. There is also a broadband continuum emitted by the hot, dense, highly ionized laser amplifier during the lasing process. This continuum is the dominant noise source in the hologram experiments. The longitudinal coherence length of the laser emission is estimated to be greater than 100 μm on the basis of the laser linewidth, if we assume a Doppler-broadened line profile with an ion temperature of 400 eV (6). The lower bound on the transverse coherence length is 3.5 μm at the end of the x-ray laser

amplifier. This is based on the measured source size of 70 μm (7) for a laser amplifier 4 cm in length. The effect of coherence brightening (8), which is the result of the high gain-length product of the laser ($gL \sim 16$, where g is the gain coefficient and L is the length of the gain region) has been ignored so that these coherence lengths are lower bounds. The transverse profile of the x-ray laser beam has a double-peaked structure with most of the energy in one of the peaks. This structure arises from refraction effects in the laser amplifier (9). The inner portion of the higher intensity peak was used to produce the holograms.

The geometry used for the holography was a modified version of the Gabor in-line geometry as shown in Fig. 1. In this geometry the x-ray beam propagates in vacuum to the multilayer x-ray mirror where it is reflected at an angle of 60 degrees to the object and the detector. The narrow bandpass (10% at 20.8 nm) of the mirror reduces the broadband continuum energy to less than 10% of the x-ray laser energy recorded at the detector. Without this reduction, the continuum emission would significantly reduce the fringe visibility in the hologram. In this geometry, forward scattered x-rays from the object become the object beam for producing the hologram. X-rays that miss the object become the reference beam. Both beams interfere at the detector and this interference produces the hologram.

The x-ray mirror consisted of a low-scatter highly polished fused silica substrate (10) and a multilayer coating of silicon and molybdenum. The measured roughness of the finished mirror was 0.07 nm (root-mean-squared) and the flatness over 100 μm was $\lambda/100$ at 20 nm (11). A scale length of 100 μm for the holograms was typical. A flatness of at least $\lambda/10$ at 20 nm (x-ray laser quality) was required in order not to destroy the coherence of the x-ray laser beam. The multilayer coating consisted of 20 alternating 9.8-nm layers of silicon and 3.0-nm layers of molybdenum. This produced a measured x-ray reflectivity of 25% for 20.8-nm light at a 60° grazing angle. The coatings were de-

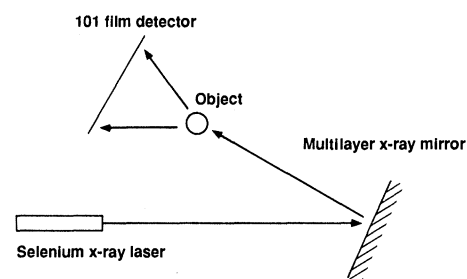


Fig. 1. Schematic arrangement of the Gabor in-line holography geometry modified by the inclusion of a narrow bandpass multilayer x-ray mirror.

Lawrence Livermore National Laboratory, Livermore, CA 94550.

signed with the LLNL computer code MLPLUS (12) and coated at Lawrence Berkeley Laboratory Center for X-ray Optics where the x-ray reflectivity was also measured.

The detector was Kodak 101 x-ray film, which has a sensitivity at this wavelength range of approximately one photon per square micrometer and a grain size of $1\ \mu\text{m}$ (13). The spatial resolution is about 5 to $10\ \mu\text{m}$. The film was protected from stray visible and ultraviolet light by a $2.3\text{-}\mu\text{m}$ -thick free-standing aluminum filter (1 cm in diameter) (14). This filter had a measured surface roughness of 0.6 nm (root-mean-squared). This ensured that filter nonuniformities did not destroy the interference produced by the coherent x-rays on the film.

The distance from the x-ray laser to the object was 3.65 m and the distance from the

object to the film was 5.08 cm. At this distance the spatial coherence of the x-ray laser, which would scale with distance according to the Van Cittert-Zernike theorem (15), was approximately $300\ \mu\text{m}$. This allowed holograms of up to a millimeter in extent to be produced. The spatial resolution of the holography system can be estimated from the resolution limits for Gabor holography (16) to be approximately $5\ \mu\text{m}$ with the dominant limitation being the film spatial resolution. The 1-cm-diameter aperture of the filter permitted several holograms to be produced in one laser shot. By using a portion of the x-ray beam where the intensity as a function of position in the beam was rapidly varying, we could obtain a variety of exposures on a single laser shot.

Two types of objects were used in the experiments. The first type was an $8\text{-}\mu\text{m}$ diameter carbon fiber. Up to five fibers were used on each laser shot. The fibers were used to generate holograms with predictable interference fringe patterns. The dimensions of the holography system were chosen to optimize the visibility of these fringe patterns and to ensure that the spatial frequency of the interference fringes did not exceed the spatial resolution of the x-ray film. The second type was a three-dimensional structure consisting of three $10\text{-}\mu\text{m}$ gold bars in an orthonormal configuration at the tip of a $40\text{-}\mu\text{m}$ glass stalk. This figure allowed more complicated three-dimensional holograms to be produced. Both objects were opaque at the x-ray laser wavelengths.

The results are shown in Figs. 2 and 3. The top portion of Fig. 2 shows the fringe pattern obtained from a carbon fiber. Four to five fringes are observed. This figure was obtained by digitizing the data with a 30 to 1 aspect ratio rectangular slit and converting the film density to linear exposure (photons per square micrometer). The density-exposure curve for the conversion was obtained from (12). The middle portion of Fig. 2 shows the average exposure as a function of transverse distance from the wire. The bottom portion of Fig. 2 shows the calculated fringe pattern for an opaque strip.

This calculated fringe pattern was obtained with the analytic results derived in a Fraunhofer diffraction calculation including the effects of a partially coherent source (17). A $70\text{-}\mu\text{m}$ -diameter uniform circular source was assumed. Plane-wave illumination was also assumed. The correction for the curvature of the wavefront is negligible. The normalized theory from (16) was scaled to agree with the experimentally measured peak amplitudes.

The agreement between theory and experiment for the wire object is good and the fringe peak positions and relative amplitude

decrease as a function of position agree well. Only at large transverse distances of order $200\ \mu\text{m}$ do theory and experiment appear to disagree. Here the spatial frequency of the predicted fringes is too large for the film spatial response and consequently the fringes are not resolved.

The results from the three-dimensional structure are shown in Fig. 3. The upper portion of Fig. 3 shows the gold bar structure on the $40\text{-}\mu\text{m}$ -diameter wire. The lower portion of Fig. 3 shows the reconstructed image of the structure obtained by illuminating its hologram with a helium-neon laser 3 m from the hologram. A real image was created 1.7 mm from the hologram with unit magnification. This image was projected with a microscope objective onto film. The $10\text{-}\mu\text{m}$ bars are just visible above the background noise in the film. The two-dimensional character of the reconstructed image arises from the large depth of field ($\sim 1\ \text{mm}$) of the holography system. Successful visible light reconstructions were also obtained from the wire holograms.

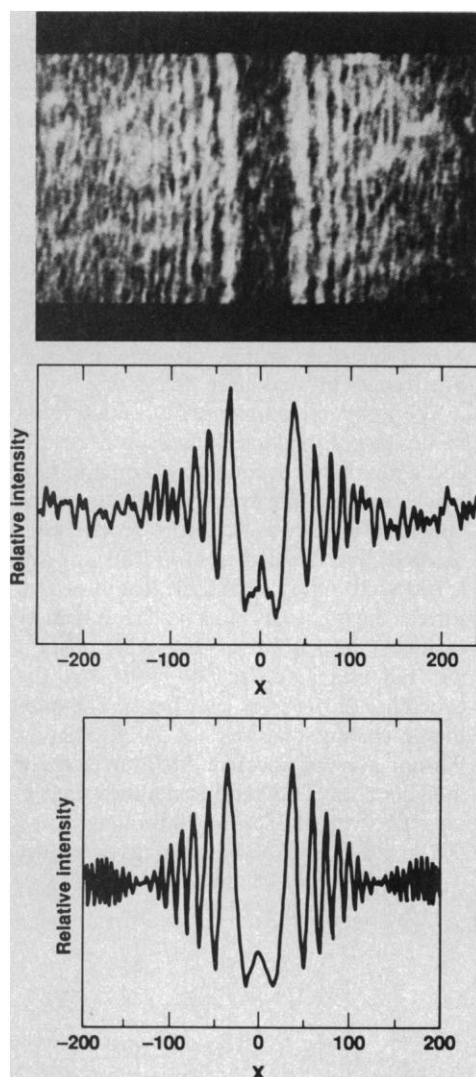


Fig. 2. X-ray hologram of an $8\text{-}\mu\text{m}$ -diameter carbon wire. (Top) Fringes obtained in the hologram on the x-ray film. (Center) The measured linear x-ray exposure as a function of relative position in the x-ray hologram. (Bottom) The predicted linear x-ray exposure as a function of position in the hologram.

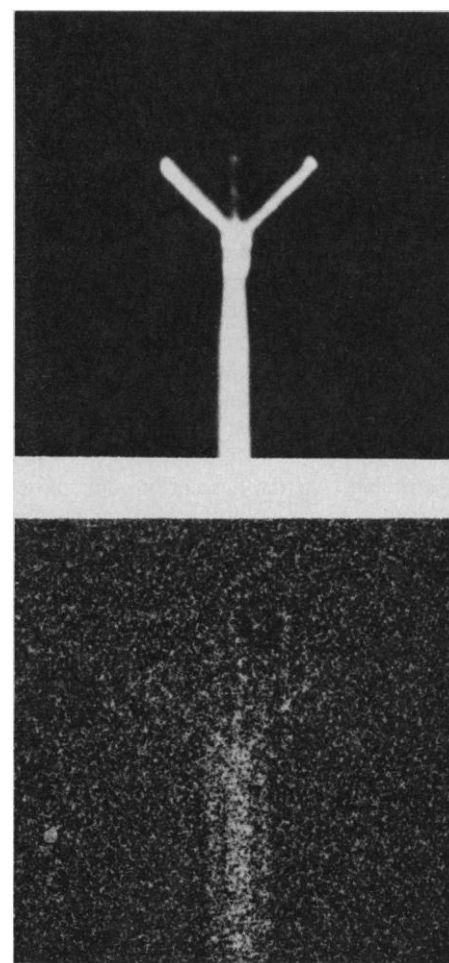


Fig. 3. (Top) A microphotograph of the three-dimensional gold bar structure used as an object. (Bottom) The reconstructed image obtained from the x-ray hologram with a visible light laser.

These experiments show that current x-ray lasers are sufficiently well-characterized and have enough brightness to be used successfully in the creation of x-ray holograms. In addition x-ray mirrors now have the necessary flatness, roughness, and reflectivities to allow their use in phase-sensitive x-ray experiments. These experiments also show that with x-ray lasers, holograms can be created with exposure times of a few hundred picoseconds. The trend in x-ray laser development is toward decreasing wavelengths and improved coherence. Lasing has been observed down as low as 6.6 nm in nickel-like europium and 5.03 nm in nickel-like ytterbium (18). This scheme should be scalable to wavelengths below 4.4 nm in nickel-like tungsten. There have been proposals for improving the spatial coherence of x-ray lasers (19). X-ray laser cavities with partially transmitting x-ray beam splitters as output couplers have also been demonstrated (20). This offers the possibility of both improved efficiency and coherence. With laser wavelengths in the water window (4.4 to 2.3 nm) where there is high contrast between protein and water, x-ray holograms of living cells can be produced.

REFERENCES AND NOTES

1. S. Aoke and S. Kikuta, *Jpn. J. Appl. Phys.* **11**, 1857 (1972).
2. M. Howells *et al.*, *Science* **238**, 514 (1987).
3. D. Gabor, *Proc. R. Soc. London Ser. A* **197**, 454 (1949).
4. T. Barbee, *Opt. Eng.* **25**, 898 (1986).
5. D. Matthews *et al.*, *Phys. Rev. Lett.* **54**, 110 (1985).
6. P. Hagelstein *et al.*, *Phys. Rev. A* **34**, 1931 (1986).
7. D. Whelan, *et al.*, in preparation.
8. A. Siegman, *Lasers* (University Science Books, Mill Valley, CA, 1986).
9. D. Matthews *et al.*, *J. Opt. Soc. B* **4**, 575 (1987).
10. The mirror substrate was fabricated by General Optics, Moorpark, CA 93021.
11. The surface measurements were performed by N. Brown and H. Bissinger of the LLNL Optics Shop. See also N. J. Brown, *Soc. Photo-Optical Instrum. Eng.* **680**, 141 (1986).
12. D. Stearns *et al.*, *ibid.* **688**, 91 (1986).
13. B. Henke *et al.*, *J. Opt. Soc. B*, **1**, 818 (1984); B. Henke *et al.*, *ibid.*, p. 828.
14. The visible and ultraviolet wavelength blocking filter was made by Luxel Corporation, Friday Harbor, WA 98250.
15. M. Born and E. Wolf, *Principles of Optics* (Pergamon, New York, ed. 3, 1986), p. 510.
16. A. Bacz, *J. Opt. Soc.* **42**, 756 (1952).
17. H. Fujiwara and K. Murata, *Opt. Acta* **19**, 85 (1972).
18. B. MacGowan *et al.*, in preparation.
19. M. Rosen, J. Trebes, D. Matthews, *Comm. Plasma Phys. Controlled Fusion* **10**, 245 (1987).
20. N. Ceglie *et al.*, in preparation.
21. We acknowledge many useful discussions with A. Szoke and M. Howells on x-ray holography and with T. Barbee on multilayer mirrors. We also wish to acknowledge J. Underwood of the Center for X-Ray Optics, Lawrence Berkeley Laboratory, for coating the x-ray mirrors and measuring their reflectivity and N. Brown and H. Bissinger of LLNL for making the surface measurements. This work was performed under the auspices of the U.S. Department of Energy by Lawrence Livermore National Laboratory under contract No. W-7405-Eng-48.

10 August 1987; accepted 9 September 1987

Release of Multiple Hormones by a Direct Action of Interleukin-1 on Pituitary Cells

EDWARD W. BERNTON, JUDITH E. BEACH, JOHN W. HOLADAY, ROBERT C. SMALLRIDGE, HENRY G. FEIN*

Exposure to bacterial endotoxins has long been known to stimulate the release of anterior pituitary hormones; administration of endotoxin was at one time a common clinical test of anterior pituitary function. Endotoxin is a potent stimulus for production of the endogenous pyrogenic protein, interleukin-1 (IL-1), by macrophages and monocytes. The possibility that IL-1 has a direct effect on the secretion of hormones by rat pituitary cells in a monolayer culture was investigated. Recombinant human IL-1 β stimulated the secretion of adrenocorticotropic hormone, luteinizing hormone, growth hormone, and thyroid-stimulating hormone. Increased hormone secretion into culture supernatants was found with IL-1 concentrations ranging from $10^{-9}M$ to $10^{-12}M$. Prolactin secretion by the monolayers was inhibited by similar doses. These concentrations of IL-1 are within the range reported for IL-1 in serum, suggesting that IL-1 generated peripherally by mononuclear immune cells may act directly on anterior pituitary cells to modulate hormone secretion in vivo. Incubation of IL-1 solutions with antibody to IL-1 neutralized these actions. These pituitary effects of IL-1 suggest that this monokine may be an important regulator of the metabolic adaptations to infectious stressors.

INTERLEUKIN-1 (IL-1), A MONOKINE secreted predominantly by stimulated macrophages and monocytes, increases the proliferation of antigen-stimulated lymphocytes and the production of lymphokines (1). In addition to these well-described effects on immune function, IL-1 also suppresses adipocyte lipoprotein lipase activity in vitro (2), stimulates hepatic synthesis of fibrinogen and iron-binding proteins (1), downregulates hepatocyte glucocorticoid receptors and gluconeogenesis (3), and increases prostaglandin production by various cells, including fibroblasts, chondrocytes, and endothelial cells (1, 4). Other hormone-like regulatory effects of IL-1 are demonstrated by its actions on the classical endocrine systems. For example, IL-1 inhibits the release of insulin from islet cells in vitro (5) and stimulates the secretion of adrenocorticotropic hormone (ACTH) and cortisol when it is injected into mice (6). IL-1 and another monokine, hepatocyte-stimulating factor, have been reported to stimulate ACTH secretion by AtT-20 cells, a mouse pituitary tumor line (7).

Although these studies showed that IL-1 has an effect on specific hormones of the pituitary-adrenal axis, the possible effects of IL-1 on other anterior pituitary hormones are unknown. Also unknown is whether the pituitary responses to IL-1 are mediated by

neuroendocrine actions on the hypothalamus or are a consequence of direct actions on pituitary cells. To address these questions, we examined the effects of recombinant human and mouse IL-1 on secretion of ACTH, luteinizing hormone (LH), prolactin (PRL), growth hormone (GH), and thyroid-stimulating hormone (TSH) by monolayers of rat anterior pituitary cells in short-term culture.

Using 3-day cultures of cells obtained from pituitaries of normal female Sprague-Dawley rats (8), we found that recombinant murine (9) and human IL-1 (10) stimulated the release of ACTH, LH, GH, and TSH. This stimulation was dose-dependent (Fig. 1). Murine IL-1 also increased the secretion of all four hormones at concentrations of $10^{-8}M$ to $10^{-10}M$, but this effect was less clearly related to dose. Prolactin secretion, in contrast, was inhibited by both murine and human IL-1 in doses of $10^{-9}M$ to $10^{-12}M$ in various experiments (Fig. 2).

Since the recombinant IL-1 preparations we used were derived from Gram-negative bacteria, it was important to establish whether these endocrine actions of our IL-1 could be a consequence of endotoxin contamination. Heat denaturing (11) completely abolished the ability of human IL-1 to alter hormone secretion from pituitary monolayers. Since this treatment would not inactivate any endotoxin contaminating the recombinant preparation, these heat-denaturing experiments demonstrate that endotoxin contaminants cannot be mediating the hormonal effects observed in these studies. Moreover, when human IL-1 was preincubated with specific antibody to recombinant

E. W. Bernton and J. W. Holaday, Division of Neuropsychiatry, Walter Reed Army Institute of Research, Washington, D.C. 20307-5100.
J. E. Beach, R. C. Smallridge, H. G. Fein, Division of Medicine, Walter Reed Army Institute of Research, Washington, D.C. 20307-5100.

*To whom all correspondence should be addressed.